IOPscience iopscience.iop.org

Home Search Collections Journals About Contact us My IOPscience

Electron inelastic mean free paths versus attenuation lengths in solids

This content has been downloaded from IOPscience. Please scroll down to see the full text.

1992 J. Phys. D: Appl. Phys. 25 262

(http://iopscience.iop.org/0022-3727/25/2/020)

View the table of contents for this issue, or go to the journal homepage for more

Download details:

IP Address: 140.113.38.11
This content was downloaded on 28/04/2014 at 18:58

Please note that terms and conditions apply.

J. Phys. D: Appl. Phys. 25 (1992) 262–268. Printed in the UK

Electron inelastic mean free paths versus attenuation lengths in solids

Y F Chen†, C M Kwei†§ and C J Tung‡

† Department of Electronics Engineering, National Chiao Tung University, Hsinchu, Taiwan, Republic of China
‡ Institute of Nuclear Science, National Tsing Hua University, Hsinchu, Taiwan, *Republic of China*

Received 1 July 1991

Abstract. The electron inelastic mean free path is of basic importance in theoretical and applied radiation physics and surface physics. It can be calculated using the dielectric function for the valence band and atomic generalized oscillator strengths for inner shells of a solid. Although the experimentally determined attenuation length is conceptually different from the theoretically calculated mean free path, they are frequently used interchangeably in a loosely defined manner. For electrons with energies below a few keV, elastic scattering plays an important role in connecting these two quantities. This work employed elastic scattering cross sections derived using the partial wave expansion method with a solid potential to evaluate the path length distribution of an electron transmitted through a solid film. Both the analytical multiple-scattering formulation and the numerical Monte Carlo simulation have been applied in this investigation. A comparison between electron inelastic mean free paths and attenuation lengths was made.

1. Introduction

Reliable information on inelastic mean free paths (IMFPs) and attenuation lengths (ALs) of low-energy electrons in solids is important in quantitative surface and interface analyses. The IMFP represents the average path length that an electron travels between two successive inelastic interactions. It can be calculated using the dielectric function for the valence band and atomic generalized oscillator strengths for inner shells of a solid. The AL is the projected distance of the IMFP along the incident electron direction. It is usually determined by neglecting elastic scatterings in an experimental overlayer method (Powell 1986, 1987, 1988). Since accurate measurements of AL for low-energy electrons are fairly difficult, it is important to estimate the AL from the calculated IMFP. Although the AL and the IMFP are frequently used interchangeably, the difference between them may reach 30% (Jablonski *et al* 1988, Jablonski and Ebel 1988).

There are several methods available for the estimation of electron elastic scattering cross sections. The main differences among these methods are the quantum mechanical approach and the assumption about scattering potentials. One of the most convenient and frequently used methods is the screened Coulomb potential within the first Born approximation. This method has been modified to incorporate it with realistic scattering potentials. Green and Leckey (1976) considered the distortion of charge density due to the lattice periodicity in the solid to modify the atomic Thomas–Fermi potential. Kwei (1984) took into account the solid state effect by considering a screened potential derived from the Hartree–Fock electron density distribution with the Wigner–Seitz boundary condition. In quantitative surface analysis, the electron energy of interest is usually less than 2 keV where the Born approximation is no longer valid. In this case, the phase shift analysis should be employed. Ichimura *et al* (1980) used a Thomas–Fermi atomic potential in the partial wave expansion method to calculate elastic scattering cross sections of electrons. In this work, we employed the screened potential associated with the Hartree–Fock–Wigner–Seitz (HFWS) electron densities (Tucker *et al* 1969) in the phase shift analysis to calculate these cross sections for low-energy electrons. We evaluated phase shifts by the WKB approach which was quite simple and accurate.

With calculated elastic differential cross sections, we then applied both the analytical multiple scattering formulation and the numerical Monte Carlo simulation to compute the path length distribution of an electron transmitted through a solid film. We found that the multiple scattering formulation is valid only for large film thicknesses where many small-angle scatterings occurred during electron transmission. For small thicknesses, this formulation overestimates the path length distribution at large path lengths and significantly underestimates it at small path lengths as compared with the corresponding results of the Monte Carlo

§ To whom all correspondence should be addressed.

0022-3727/92/020262 + 07 $04.50 © 1992 IOP Publishing Ltd

simulation. We further estimated the difference between the IMFP and the AL. Our results have been compared with data given in other works.

2. Theory

2.1. Elastic scattering cross sections

The Born approximation is valid for elastic scattering cross sections of electrons with energies above about $15Z^2$ eV (Bethe and Jackiw 1968), where Z is the atomic number of the medium. The differential cross section with respect to the scattering angle θ is given by

$$\frac{d\sigma}{d\Omega} = \frac{4}{q^4}[Z - F(\boldsymbol{q})]^2 \tag{1}$$

where q is the momentum transfer, $d\Omega = 2\pi(\sin\theta)d\theta$ is the differential solid angle in the direction of the scattered electron, and $F(\boldsymbol{q})$ is the atomic form factor. Note that all quantities and expressions in this paper are in atomic units unless otherwise specified. The elastic scattering form factor of the atom is given by

$$F(\boldsymbol{q}) = \int d^3x \exp(i\boldsymbol{q}\cdot\boldsymbol{x})n(\boldsymbol{x}) \tag{2}$$

where $n(\boldsymbol{x})$ is the electron density distribution of the atom. For elastic scatterings, one may assume $q = 2k\sin(\theta/2)$, where k is the incident electron momentum.

Using a screened Coulomb potential to account for the shielding of the nuclear charge by orbital electrons in the atom, the differential cross section becomes

$$\left[\frac{d\sigma}{d\Omega}\right]_{sc} = \frac{4Z^2}{(q^2 + r_a^{-2})^2} \tag{3}$$

where r_a is the effective screening distance. Employing the Thomas–Fermi electron density distribution, it is found that r_a is roughly proportional to $Z^{-1/3}$ for moderately heavy atoms (Schiff 1968). For light atoms it is more accurate to calculate $F(\boldsymbol{q})$ by the self-consistent Hartree–Fock electron density distribution. Substituting this distribution into equations (1) and (2), we obtain

$$\frac{d\sigma}{d\Omega} = \left(Z - 2\pi\int_0^\infty r\sin[2(2E)^{1/2}\sin(\theta/2)r]n(r)\,dr\Big/ (2E)^{1/2}\sin(\theta/2)\right)^2 \Big/ 16E^2\sin^4(\theta/2) \tag{4}$$

where $E = k^2/2$ is the electron kinetic energy. The integral term in equation (4) represents the screening of the nuclear charge by atomic electrons with the density distribution $n(r)$. For a solid atom one may apply the HFWS electron density distribution and replace the upper limit in the integration by the Wigner–Seitz radius r_{WS}.

For electron energies below the Born threshold, i.e. $15Z^2$ eV, equation (1) becomes invalid. At these energies, one should apply the phase shift analysis method. The differential scattering cross section is given by

$$\frac{d\sigma}{d\Omega} = \frac{1}{4E}\left|\sum_{l=0}^{\infty}(2l+1)[\exp(2i\delta_l - 1)]P_l(\cos\theta)\right|^2 \tag{5}$$

where δ_l is the lth phase shift and $P_l(\cos\theta)$ is the Legendre polynomial of order l. Given a suitable scattering potential, the phase shifts can be calculated by an integration of the radial wave equation. Since the WKB approach is quite simple and accurate (Jochain 1975, Salvat *et al* 1985) in evaluating these phase shifts, we adopt it in this work. This approach gives the lth phase shift as

$$\delta_l(k) = (l + \tfrac{1}{2})\pi/2 - kr_0 + \int_{r_0}^{\infty} dr\{[k^2 - U^{eff}(r)]^{1/2} - k\} \tag{6}$$

where $U^{eff}(r) = l(l+1)/r^2 + V(r) + r^2/4$, $V(r)$ is the scattering potential, and r_0 is the largest zero of $k^2 - U^{eff}(r)$.

A suitable potential is required in equation (6) in order to calculate the phase shifts. This potential should give rise to the correct electron density distribution in the solid. Applying the HFWS electron density distribution for a solid atom, the potential may be given by

$$V(r) = -Z/r + \frac{1}{r}\int_0^r 4\pi r'^2 n(r')\,dr' + \int_r^{r_{WS}} 4\pi r' n(r')\,dr'. \tag{7}$$

Since the polarization effect is very small for electron energies above 100 eV, we neglect the influence of the polarization potential in this work.

2.2. Path length distribution

The paths of an energetic electron in a solid may be simulated by the Monte Carlo method. This method selects a number from a collection of random numbers to determine the scattering point, using the calculated elastic mean free path. Another number from this collection determines, from the calculated differential cross section, the angular deflection caused by this scattering. These determinations continue in a computer until the incident electron emerges from the solid. Electron trajectories and path lengths are all recorded. The calculation is repeated over and over until a statistically reliable result has been reached. Since scattering events are independent, the electron trajectory may be described by a Poisson stochastic process. The step path length is therefore given by (Murata 1974, Salvat and Parallada 1984a)

$$\Delta s = -\lambda_e \ln(R) \tag{8}$$

where R is the random number, λ_e is the elastic mean

free path given by (Salvat and Parallada 1984b, Shimizu et al 1976)

$$\frac{1}{\lambda_e} = N \int \frac{d\sigma}{d\Omega} d\Omega \tag{9}$$

and N is the number of target atoms per unit volume. To determine the angular deflection of the electron after each scattering, the elastic differential cross section is converted into a probability distribution function by dividing this cross section integrated up to a certain scattering angle by the total elastic cross section. A second random number is then picked for this determination.

An alternative way to estimate the path-length distribution of an electron is to solve the Boltzmann transport equation. Yang (1951) derived this distribution using the multiple scattering approximation which assumed many small-angle scatterings contributing to the final deflection of the electron. He found that the probability distribution of the path-length might be expressed in terms of a dimensionless variable v as

$$F(v)=\begin{cases} 2\pi^{-1/2}v^{-3/2}[\exp(-1/v)-3\exp(-9/v)] & v<2 \\ \pi\exp(-\pi^2 v/16)/4 & v\geq 2 \end{cases} \tag{10}$$

where $v = 2(s-t)/\langle s-t\rangle$, s is the path length, t is the depth of penetration or the thickness of the film, and $\langle s-t\rangle$ is the average increase in path-length over the depth of penetration. The path-length distribution $F(t,s)$ may be calculated using the relation $F(t,s)\,ds = F(v)\,dv$. In this work, we computed this distribution using equation (10) with the parameter $\langle s-t\rangle$ obtained from the Monte Carlo calculation. In addition, we applied the direct Monte Carlo simulation to compute the same distribution. By comparison, we found that the multiple scattering approximation was useful only for high-energy electrons and large penetration depths.

2.3. IMFP versus AL

The assumption of an equivalence for the measured AL and the calculated IMFP is an over simplification. As shown in figure 1, an electron with incident angle α with respect to the surface normal passes through a solid film of thickness t. Since elastic scatterings modify electron trajectories from straight paths, the total path-lengths s, a sum of segmental path-lengths or $s_1 + s_2 + s_3 + \ldots$, is greater than the penetration depth t. To determine the AL, the film thickness should not be more than a few IMFPs. Since the elastic mean free path is several times smaller than the IMFP (see figure 5 later), plural scatterings or even multiple scatterings occur during the electron transmission. The AL is usually determined by analysing the zero-energy loss peak of the transmited spectrum of a normal incident electron. As shown in figure 1, the transmitted electron emerges from the film with a lateral displacement x and at an exit angle β with respect to the surface normal. Since the occurrence of scattering events obeys the Poisson stochastic process, the ratio of the zero-loss transmission electron intensity to the incident electron intensity is described by $\exp(-s/\lambda_i)$, where λ_i is the IMFP. The IMFP can be calculated using the dielectric function of the solid (Pines 1964, Tung and Ritchie 1977, Ashley et al 1979, Tung et al 1979).

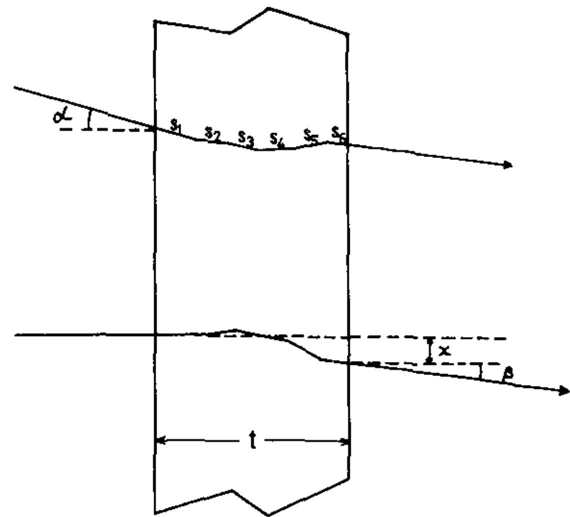

Figure 1. An electron with incident angle α (upper sketch) with respect to the surface normal passes through a solid film of thickness t. After several elastic scatterings resulting in the total path length $s = s_1 + s_2 + s_3 + \ldots$, this electron emerges from the film. Another normally incident electron (lower) passes through the film with an exit angle β with respect to the surface normal and with a lateral displacement x.

The relation between the IMFP and the AL is thus given by

$$\int F(t,s)\exp(-s/\lambda_i)\,ds = \exp(-t/\lambda_a\cos\alpha) \tag{11}$$

where λ_a is the AL. if we neglect elastic scatterings, i.e. substituting $F(t,s) = \delta(s - t/\cos\alpha)$ into equation (11), we obtain $\lambda_i = \lambda_a$ as it should be. Equation (11) reveals that the probability of an electron escaping with zero-energy loss from the film drops to e^{-1} of its original value at $t = \lambda_a$ for $\alpha = 0$ and to zero for $\alpha = \pi/2$.

3. Results and discussion

Figure 2 shows some representative results of the elastic scattering differential cross section as a function of scattering angle for electrons of several energies in aluminium. These cross sections were calculated using equations (5)–(7). It is seen that elastic scatterings are predominantly in the forward direction with enhanced small-angle scatterings for high-energy electrons. In figure 3 we plot the ratio of the elastic differential cross section calculated using the Born approximation (BN) to that using the phase shift method (PS) for electrons of several energies in aluminium. The broken curves represent results of the Thomas–Fermi screened Coulomb potential for the free atom. The full curves are

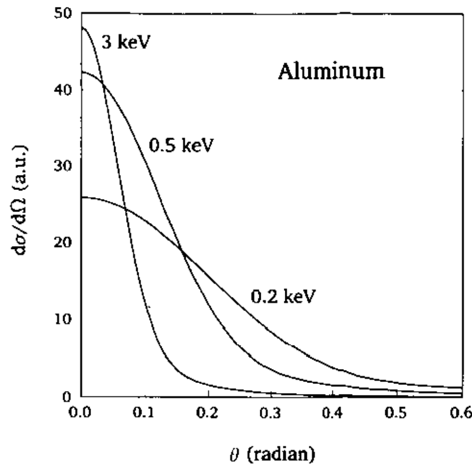

Figure 2. A plot of elastic scattering differential cross section for different energy electrons in aluminium as a function of scattering angle.

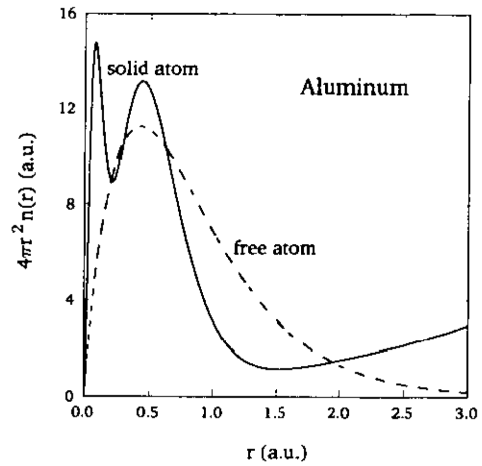

Figure 4. The electron density distribution associated with free (broken curve) and solid (full curve) atomic potentials in aluminium.

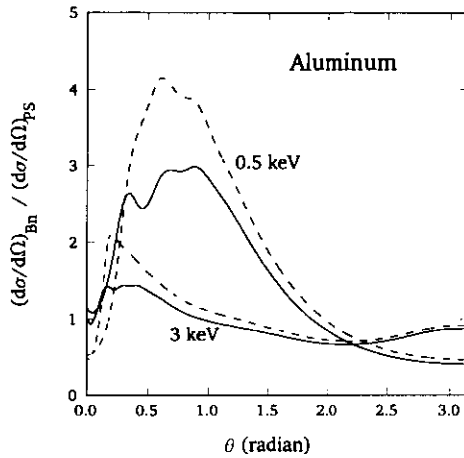

Figure 3. The ratio of elastic differential cross section in aluminium calculated using the Born approximation with different potentials to that using the phase shift method. Broken curves represent results for the free atomic potential. Full curves correspond to those of the solid atomic potential.

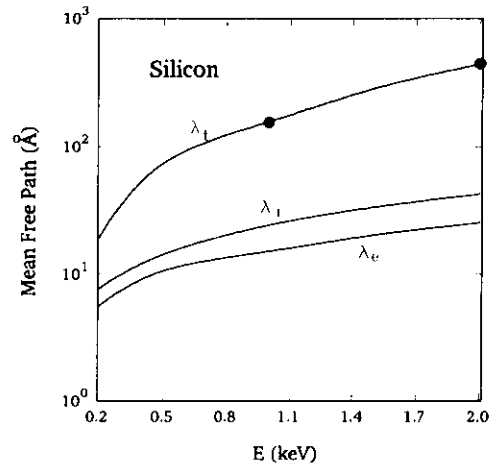

Figure 5. A plot of the various electron mean free paths in silicon as a function of electron energy. Here λ_i, λ_e and λ_t represent the inelastic, elastic and transport mean free paths, respectively. Data on λ_t taken from Tofterup (1985) are included for comparison.

those corresponding to the solid atom using the HFWS potential. It reveals that this ratio approaches unity at large scattering angles for high-energy electrons. At small angles the Born approximation overestimates the differential cross section to some degree depending on the electron energy. This overestimation is remarkable for electron energies below the Born threshold. Electron density distributions associated with the screened Coulomb potential for both the free and the solid aluminium atoms are plotted in figure 4. Again, the Thomas–Fermi and the HFWS potentials were employed for the free and the solid atoms respectively. Note that small-angle scatterings correspond to large impact parameters where the nuclear charge screening by atomic electrons is high. Since the electron density extends to infinite radius for free atoms but to Wigner–Seitz radius for solid atoms, the differential cross section for small-angle scatterings is thus larger for free atoms than for solid atoms.

In figure 5 we plot the various electron mean free paths in silicon as a function of incident electron energy. The inelastic mean free path λ_i was calculated using experimental optical data fitted to the Lindhard dielectric function (Tanuma *et al* 1988). The elastic mean free path λ_e was computed using equations (5)–(7) and (9). The transport mean free path λ_t, defined by

$$\frac{1}{\lambda_t} = N \int (1 - \cos\theta) \frac{d\sigma}{d\Omega} d\Omega \qquad (12)$$

is a measure of the effectiveness of elastic scatterings in causing the deflection of electrons. It is seen from figure 5 that λ_e is smaller than λ_i for all electron energies. The difference between λ_e and λ_t is due to the cosine term in equation (12). The significant difference

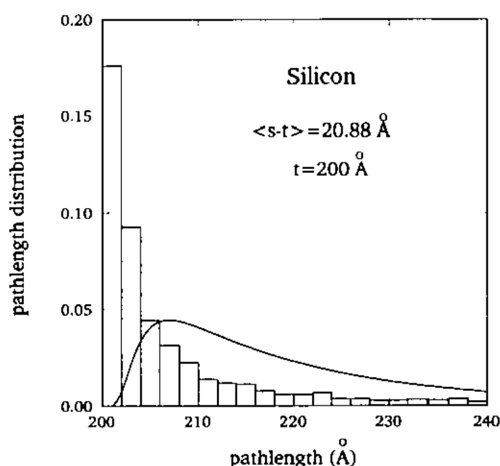

Figure 6. The path-length distribution for electrons of 1.5 keV passing through a silicon film of 200 Å. Histograms represent the Monte Carlo results. The full curve corresponds to the multiple scattering distribution.

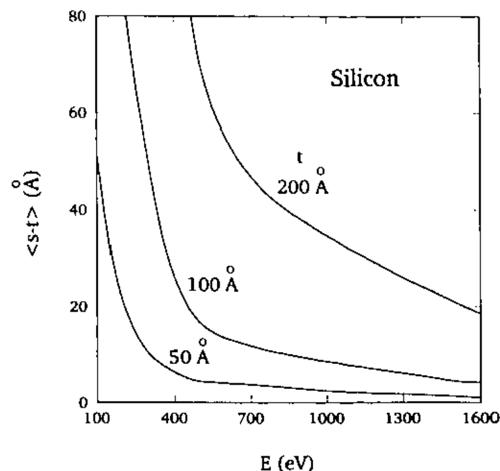

Figure 8. The average increase in path-length over the depth of penetration for electrons passing through silicon films of several thicknesses.

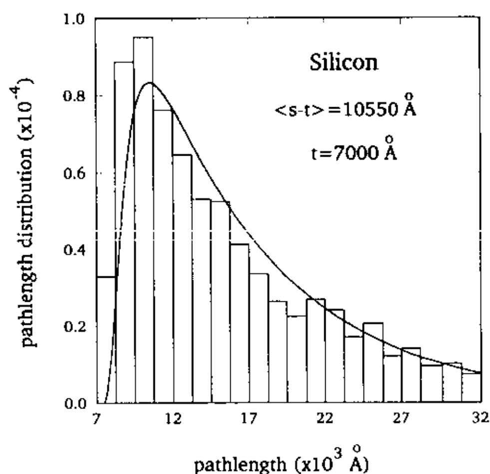

Figure 7. The path-length distribution for electrons of 1.5 keV passing through a silicon film of 7000 Å. Histograms represent the Monte Carlo results. The full curve corresponds to the multiple scattering distribution.

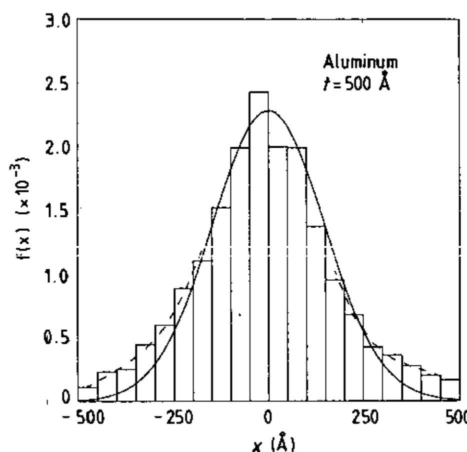

Figure 9. Monte Carlo results of the distribution in lateral displacement of electrons emerging from an aluminium film of 500 Å thickness. The full curve is the multiple scattering Gaussian peak. Broken curves are the single scattering tails at large displacements.

shown indicates that elastic scatterings are predominantly in the forward direction. Data on λ_t taken from other work (Tofterup 1985) are included in figure 5 for comparison.

A plot of the path-length distribution calculated using the multiple scattering formula of equation (10) and using the Monte Carlo method for an electron of 1.5 keV energy passing through a silicon film of 200 Å thickness is shown in figure 6. A comparison of these results shows that the multiple scattering formula overestimates the distribution at large path-lengths but significantly underestimates it at small path-lengths. This may be understood as due to the multiple scattering approximation which assumes the occurrence of many small-angle scatterings during the electron transmission. Since in this case the film thickness is only about ten times the elastic mean free path (see figure 5), plural scatterings (i.e. less than about 100 scatterings) rather than multiple scatterings occur most often. The small number of scatterings results in small angular deflections and consequently small path-lengths. Indeed, the relative difference between the average path-length (220.88 Å) and the penetration depth (200 Å) is only about 10%. A similar plot of this distribution for the 7000 Å silicon film is shown in figure 7. In this case the relative increase in the average path-length (17 550 Å) over the penetration depth (700 Å) reaches 150%. Thus, the path-length distribution calculated using the multiple scattering formula agrees quite well with that using the Monte Carlo method. It is seen that this distribution is asymmetric with the most probable value much smaller than the mean value due to the predominance of small-angle scatterings. Further, the path-length distribution evolves from a delta function for zero film thickness (Tougaard and Sigmund 1982) to broader and broader distributions for increased thicknesses. In figure 8 we

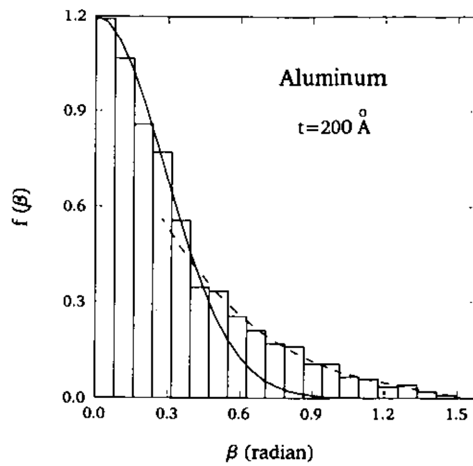

Figure 10. Monte Carlo results of the angular distribution of electrons emerging from an aluminium film of 200 Å thickness. The full curve is the multiple scattering Gaussian peak. The broken curve is the single scattering tail at large exit angles.

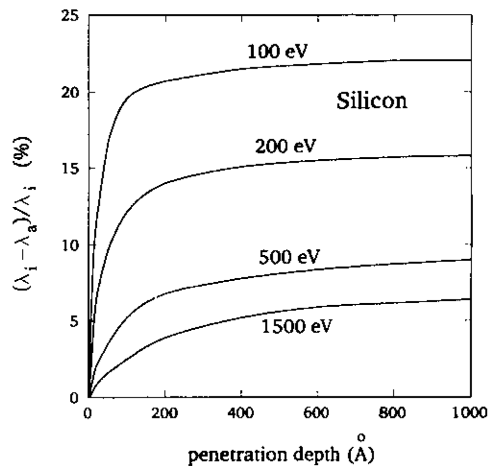

Figure 11. A plot of the relative difference between the IMFP and AL for electrons of several energies in silicon.

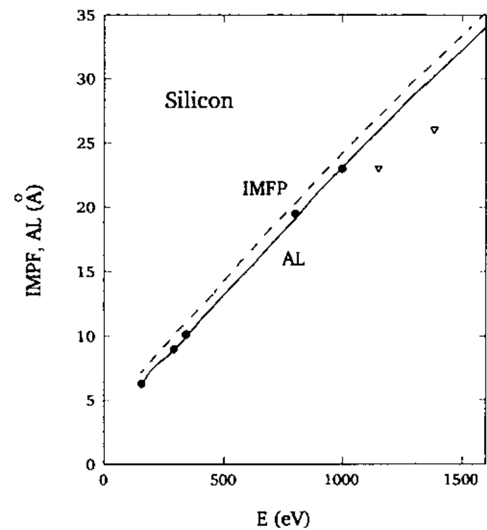

Figure 12. A comparison of IMFP and AL for electrons in silicon. The full curve is the results of present calculation in AL. The broken curve is the data of Tanuma *et al* (1988) in IMFP. The points are experimental AL data of: circles, Zaporozhchenko *et al* (1979); triangles, Flitsch and Raider (1975).

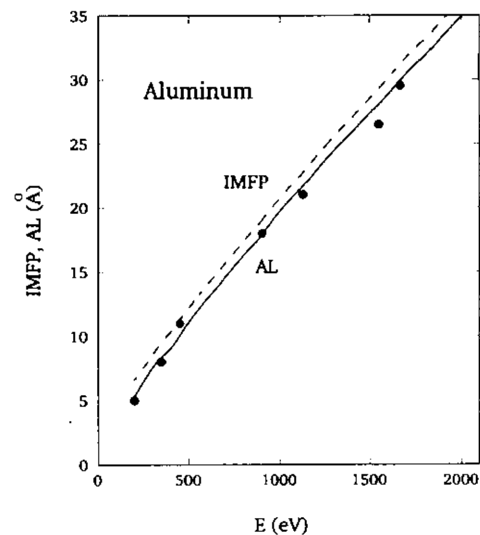

Figure 13. A comparison of IMFP and AL for electrons in aluminium. The full curve is the results of present calculation in AL. The broken curve is the data of Ashley *et al* (1979) in IMFP. The points are experimental AL data of Tracy (1974).

plot the average increase in path-length over the depth of penetration for electrons passing through silicon films of different thicknesses. For a fixed electron energy, the increase is enhanced for larger thicknesses owing to the increased number of elastic scatterings. Similarly, this increase falls with increasing electron energy for a fixed thickness.

Variations in the exit angle β and the lateral displacement x of electrons emerging from the film (see figure 1) are also of interest. According to the electron scattering theory in a thin film (Jackson 1975, Bethe and Ashkin 1953), these two distributions are strongly correlated. They exhibit structures consisting of two components, i.e. the multiple scattering Gaussian peak and the single or plural scattering tail. Figure 9 shows a plot of Monte Carlo results for the distribution in lateral displacement of electrons passing through an aluminium film of 500 Å thickness. For comparison we also plot the fitted multiple scattering Gaussian peak and the single scattering tail distributions. A plot of the angular distribution for electrons transmitted through an aluminium film of 200 Å thickness is shown in figure 10. Again, the small-angle scattering Gaussian peak and the wide-angle single scattering distribution are also included for comparison. It is seen that the transition from multiple to single scattering occurs at $\beta \approx 0.4$. At this point, the angular distribution divides itself into two roughly equal portions. This indicates that the contribution from multiple and single scattering is about the same.

By substituting the calculated path length distributions into equation (11), we calculated attenuation lengths of electrons. A plot of the relative difference between the IMFP and the AL as a function of silicon film thickness for several electron energies is plotted in figure 11. It is seen that below about 200 Å this difference increases rapidly with the penetration depth and then begins to saturate at larger penetration depths. For a fixed penetration depth, this difference increases with decreasing electron energy. This is consistent with the results of the differential cross section shown in figure 2, where smaller electron energies exhibit larger cross sections for large scattering angles. The ratio of AL to IMFP for sufficiently large penetration depths agrees with the data of Jablonski (1987) who derived λ_a/λ_i as 0.753 and 0.926 for Auger electrons of 92 eV and 1619 eV, respectively.

Figures 12 and 13 show a comparison of IMFP and AL for electrons in silicon and aluminium, respectively. The IMFP values of Tanuma *et al* (1988) and Ashley *et al* (1979) were used in the computation of AL using equation (11). Experimental AL data for silicon (Zaporozhchenko *et al* 1979, Flitsch and Raider 1975) and aluminium (Tracy 1974) are included for comparison. It is seen that the present calculated AL results are in good agreement with the measured data.

4. Conclusion

Elastic scatterings are responsible for the differences between IMFP and AL and between electron path-length and penetration depth. In this work we have dealt with these differences by applying elastic differential cross sections to the multiple scattering formulation and to the Monte Carlo simulation. These cross sections have been evaluated using the partial wave expansion method with phase shifts calculated by the WKB approach and the HFWS electron density distribution. Our approach yielded good results to account for these differences. Calculations performed in this work indicated that these differences were dependent on electron energy and penetration depth.

The path length distribution, the angular distribution and the distribution in lateral displacement of electrons emerging from a solid film showed that the multiple scattering approximation worked quite well for large penetration depths and high-energy electrons. On the contrary, the single or plural scattering dominated the contribution to these distributions. The transition from multiple scattering distributions to single scattering distributions occurred at different values of the angle and the lateral displacement, depending on the film thickness and the electron energy.

Acknowledgment

This research was supported by the National Science Council of the Republic of China.

References

Ashley J C, Tung C J and Ritchie R H 1979 *Surf. Sci.* **81** 409
Bethe H A and Ashkin J 1953 *Experimental Nuclear Physics* ed E Segre (New York: Wiley) p 282
Bethe H A and Jackiw R W 1968 *Intermediate Quantum Mechanics* (New York: Benjamin)
Flitsch R and Raider S I 1975 *J. Vac. Sci. Technol.* **12** 305
Green A J and Leckey R C G 1976 *J. Phys. D: Appl. Phys.* **9** 2123
Ichimura S, Aratama M and Shimizu R 1980 *J. Appl. Phys.* **51** 2853
Jablonski A 1987 *Surf. Sci.* **188** 164
Jablonski A and Ebel H 1988 *Surf. Interface Anal.* **11** 627
Jablonski A, Krawczyk M and Lesiak B 1988 *J. Electron Spectrosc.* **46** 131
Jackson J D 1975 *Classical Electrodynamics* (New York: Wiley) p 647
Jochain C J 1975 *Quantum Collision Theory* (Amsterdam: North-Holland)
Kwei C M 1984 *Thin Solid Films* **111** 83
Murata K 1974 *J. Appl. Phys.* **45** 4110
Pines D 1964 *Elementary Excitations in Solids* (New York: Benjamin)
Powell C J 1986 *J. Vac. Sci. Technol.* A **4** 1532
—— 1987 *Surf. Interface Anal.* **10** 349
—— 1988 *J. Electron Spectrosc.* **47** 197
Salvat F, Mayol R, Molins E and Parallada J 1985 *J. Phys. D: Appl. Phys.* **18** 1404
Salvat F and Parallada J 1984a *J. Phys. D: Appl. Phys.* **17** 185
—— 1984b *J. Phys. D: Appl. Phys.* **17** 1545
Schiff L I 1968 *Quantum Mechanics* (New York: McGraw-Hill)
Shimizu R, Kataoka Y, Ikuta T, Koshikawa T and Hashimoto H 1976 *J. Phys. D: Appl. Phys.* **9** 101
Tanuma S, Powell C J and Penn D P 1988 *Surf. Interface Anal.* **11** 577
Tofterup A L 1985 *Phys. Rev.* B **32** 2808
Tougaard S and Sigmund P 1982 *Phys. Rev.* B **25** 4452
Tracy J C 1974 *J. Vac. Sci. Technol.* **11** 280
Tucker T C, Roberts L D, Nestor C W and Carson T A 1969 *Phys. Rev.* **178** 998
Tung C J, Ashley J C and Ritchie R H 1979 *Surf. Sci.* **81** 427
Tung C J and Ritchie R H 1977 *Phys. Rev.* B **16** 4302
Yang C N 1951 *Phys. Rev.* **84** 599
Zaporozhchenko V I, Kalafati Y D, Kukharenko Y A and Sergeev V M 1979 *Izv. Akad. Nauk SSSR. Ser. Fiz.* **43** 199